Towards Development of a Snow Water Equivalence (SWE) Algorithm Using Microwave Radiometry over Snow Covered First-Year Sea Ice

Sheldon D. Drobot and David G. Barber

Abstract

In this paper we investigate snow geophysical and microwave radiometric sensor characteristics (frequency, incidence, and polarization) as they pertain to the development of a snow water equivalence (SWE) algorithm for first-year sea ice. Physical and electrical snow properties and in situ microwave radiometry (19, 37, and 85 GHz; V and H polarization) data were collected during a 36-day period in early 1996 under the Collaborative-Interdisciplinary Cryospheric Experiment (C-ICE).

Density, liquid water content, and salinity varied significantly over the snow volume vertical dimension. Diurnal sampling indicated a difference in liquid water content. Corresponding changes in salinity and density were not detected. Within the framework of this case study, 37-GHz H polarization was the most precise single frequency for SWE estimation. Multiple regression techniques show promise as an effective avenue to pursue the development of SWE algorithms.

Introduction

The polar environments will likely be the first to indicate signs of climatic change because of their sensitivity to subtle changes occurring within the global climate through a variety of enhanced feedback processes. For instance, the well documented sea ice-albedo feedback mechanism is thought to account for a considerable amount of projected climatic warming at high latitudes (Rind *et al.*, 1995). The basic concept is that increasing atmospheric temperatures will cause a reduction in the spatial and temporal extent of sea ice at any particular location. Significantly lower albedos at the surface will result, "feeding back" an amplification of the original atmospheric warming, thereby enhancing the atmospheric temperature change.

Confusion remains surrounding the spatial and temporal variation of snow cover under changing climatic conditions. Snow is an integral component of the ocean-sea ice-atmosphere interface. Its thermodynamic and geophysical characteristics significantly affect a host of physical and biological processes. Work by Brown and Cote (1992) has shown that snow thickness was a significant determining factor in interannual first-year sea ice thickness. Ledley (1991; 1993) indicated a thicker snow cover could retard sea ice ablation, thereby having a net cooling effect (in fact, resulting in a negative feedback). However, recent empirical (Brown and Goodison, 1993) and model (Flato and Brown, 1996) results show a more complex pattern that may not agree with the results of Ledley (1993).

Uncertainty surrounding the physical processes operating across the ocean-sea ice-atmosphere interface, and poor climatological information on snow distributions over sea ice, has lead to considerable research emphasis focusing on determining snow distributions remotely. In particular, efforts to monitor snow are being expended using frequencies spanning the full range of the electromagnetic (EM) spectrum. Research to date suggests that microwave frequencies are the most likely candidates for estimating the snow water equivalence (SWE) over sea ice (Goodison, 1995). Gamma radiation approaches are used operationally for SWE estimation over terrestrial surfaces (Carroll, 1990) but are not available on satellite platforms. Microwave radiometry is also used operationally for estimation of terrestrial SWE (Walker and Goodison, 1993) but not over sea ice surfaces. Researchers have also used optical and UV frequencies for estimation of various physical characteristics of snow covers (e.g., grain size, density, particulate inclusions, etc.), and optical and active microwave sensors are routinely used to map snow pack presence and ablation state as inputs to hydrological models (Rango, 1988).

The theoretical framework for microwave scattering over snow covered sea ice is a reasonably mature science (Carsey, 1992). The conceptual underpinnings for SWE estimation with microwave radiometry are based on the effect that a snow layer has on microwave emission originating within the underlying sea ice. Thicker and denser snowpacks increase the effective complex permittivity of the material, resulting in an increase in volume scattering and a decrease in the apparent microwave brightness temperature (T_B). Horizontal (H) polarization is thought to be more sensitive to snow depths if melt-freeze metamorphism has occurred (Foster *et al.*, 1984), but practical studies have shown vertical (V) polarization to be equally effective as a SWE estimator (e.g., Goodison *et al.*, 1990). Empirical results to date substantiate

S.D. Drobot is with the Department of Geography, University of Nebraska-Lincoln, Lincoln, NE 68588-0135 (sdrobot@unlgradl.unl.edu).

D.G. Barber is with the Centre for Earth Observation Science, Department of Geography, University of Manitoba, Winnipeg, Manitoba R3T 2N2, Canada (dbarber@ms.umanitoba.ca).

Photogrammetric Engineering & Remote Sensing, Vol. 64, No. 5, May 1998, pp. 415–423.

0099-1112/98/6405–415$3.00/0

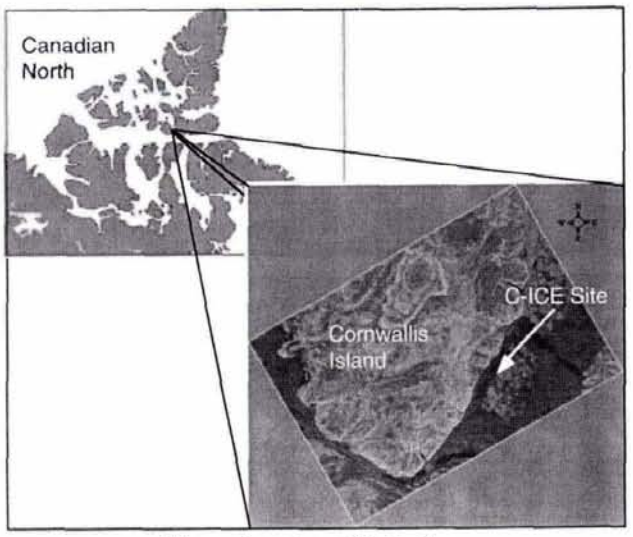

Figure 1. C-ICE '96 field site.

theoretical models through correlation analyses between SWE values and the T_B (Chang *et al.*, 1982; Kunzi *et al.*, 1982; Grenfell and Lohanick, 1985; Comiso *et al.*, 1989; Lohanick, 1993).

Complications in this relationship occur with the inclusion of liquid water in the snow volume (Goodison, 1995), or with varying grain size (Mätzler, 1997). Water in liquid phase not only alters the complex permittivity of the snowpack but the water also becomes a microwave emitter. This complicates the T_B-SWE relationship derived for dry snow because the volume scattering losses are now compounded from emission within the snow volume as well as the sea ice. As a result, the principle of using volumetric scattering for SWE estimation no longer applies. Grain geometry is not as well understood, but results indicate that the grain size may also be very important in understanding changes in the T_B (Chang *et al.*, 1976; Hall *et al.*, 1986; Mätzler, 1997).

Our objectives in this paper are to investigate the relationship between SWE and microwave emission through an evaluation of the *in situ* physical and electrical properties which give rise to this connection. We will specifically focus on the co-occurrence of brightness temperatures at 50° (near Special Sensor Microwave/Imager incidence angle) and the diurnal and seasonal evolution of the snow. Our intention is to investigate the statistical relationships between T_B and SWE and to explain these empirical results by assessing the physical and electrical characteristics which drive this relationship. We see this as a requisite step in the formulation and testing of candidate algorithms which would exploit spaceborne passive microwave sensors for SWE estimation over snow covered sea ice.

Methods

Data were collected as part of the Collaborative Interdisciplinary Cryosphere Experiment (C-ICE '96) from 11 May to 15 June 1996. The field site was located approximately 70 km northeast of Resolute Bay, Cornwallis Island, Northwest Territory, Canada (Figure 1).

Snow and Sea Ice Sampling

Physical Properties

Snow profiles were collected from an area adjacent to the radiometer site (Figure 2). Sampling was performed without replacement in a 0.375-m² "crystal pit." All measurements were taken on the diffusely illuminated snow wall (perpendicular to the solar disk) in order to minimize the effect of solar insolation. Data were gathered three times daily, at approximately 7:30 AM (*am*), 1:30 PM (*noon*), and 6:30 PM (*pm*) CST.

During each measurement set, snow depth, density, volumetric liquid water content, ice surface and snow salinity, and ice and snow temperatures were recorded. Depth was recorded to the nearest half cm with a metre stick. Density samples were removed at 2-cm vertical intervals with a 66.36-cc density cutter and placed into a sealed plastic bag. Each sample was then weighed to the nearest 10th of a gram on a digital scale, and subsequently converted to $kg \cdot m^{-3}$ using the gravimetric technique. We estimate the precision of this approach to be within $\pm$ 40 $kg \cdot m^{-3}$ based on replicate sampling and previously published results (Garrity and Burns, 1988). The percent water in liquid phase was estimated with a capacitance plate (dielectric device). Values were recorded from the plate at intervals of 1 m above the snow surface (relative calibration to air), on the snow surface, and at the midpoint of each 2-cm snow sample on the pit wall. The 0- to 6-cm layers above the ice surface contain brine, which negates the capacitance approach to estimating liquid water content. In these basal layers, we estimated the free water content by extrapolation based on the values observed in the brine-free layers of the upper snow pack. Snow salinity was measured by melting the snow density samples to room temperature and measuring bulk salinity using an optical refractometer. Ice surface salinity was measured by scraping the top 2 mm of the ice surface for measurement using the optical refractometer. Snow temperature data were recorded continuously as 15-minute averages by Campbell Scientific Instruments data loggers (model 21X). In this research, we use snow and ice temperatures measured with 24 AWG, Cu-Co thermocouple junctions. The junctions were embedded in brass tubing (9 by 0.5 cm) which, in turn, were fastened at predetermined levels to a wooden dowel. Temperatures were measured at a 3-cm vertical spacing through the snow and at depths of 1 cm, 4 cm, 10 cm, and 40 cm from the snow-ice interface through the sea ice volumes. The sensor arrays (including leads) were painted white to minimize thermal contamination. The snow was packed evenly during backfilling and the sensor leads, which extended to the data logger, were buried to further minimize thermal contamination. Additional details of these methods are presented elsewhere (Barber *et al.*, 1994; Barber *et al.*, 1995).

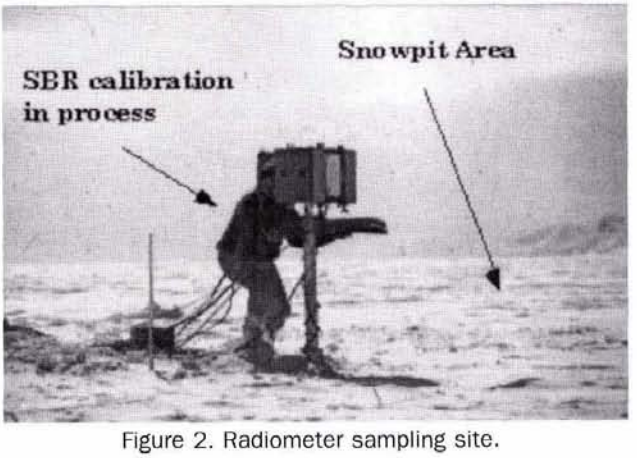

Figure 2. Radiometer sampling site.

Physical properties of the snowpack were subsequently divided into six layers for analysis purposes. Layers containing brine, at 2 cm, 4 cm, and 6 cm, were unaltered, due to the significant effect the salinity has on dielectrics. The remaining snowpack was stratified into three equal segments. Layering the snowpack in this manner allowed us to make meaningful intercomparisons between days with different snow depths.

Electrical Properties

Electrical properties of the snowpack were derived using the *in situ* physical and temperature data. In this work, the complex dielectric constant, expressed as $\varepsilon = \varepsilon' - j\,\varepsilon''$, where $j = \sqrt{-1}$, is used to describe the electrical characteristics of the snowpack. Permittivity, ε', characterizes the relative permittivity with respect to free space ($\varepsilon'_{air} = 1$), while the dielectric loss, ε'', defines the electromagnetic loss of the material. Permittivity describes what happens to EM energy when it impinges upon a boundary. Loss describes the electromagnetic loss once energy has penetrated into the material. The total electromagnetic loss (Hallikainen and Winebrenner, 1992) is a combination of absorption loss (transformation of energy into another form) and scattering loss (energy deflected to travel in directions other than incident).

The dielectric constant of dry snow is governed by the electrical properties of ice, the snow density, snow crystal geometry, and frequency. From 10 MHz to 1000 GHz, the permittivity of dry snow, ε'_{ds}, is independent of temperature between 0 to −18°C (Cumming, 1952). Therefore, ε'_{ds} is regulated only by snow density. Although the theoretical limit of ε'_{ds} is 3.17 (the value of pure ice), natural variation in snowpack density is generally within 200 to 500 kg·m^{-3}, resulting in ε'_{ds} values of 1.4 to 2.0. Loss values are largely dependent on salinity, which is significant in the basal layer of snow covers on first-year sea ice (Barber *et al.*, 1995), and on wetness.

Wet snow electrical properties are regulated by volumetric water content, snow density, the geometry of ice and water inclusions, and frequency. The presence of water substantially increases both the permittivity and loss of the medium, because the effective complex permittivity of water is significantly higher than ice or air.

Modeled parameters used in these analyses include the fractional volumes of air, ice, and brine, and the complex dielectric constant of the snow cover. The fractional volumes were computed based on the observed density, salinity, and temperature of the snow. The dielectric constant was modeled using various forms of the Debye equations, depending on the nature of the partial fractions of ice, air, brine, and water in liquid phase. When brine was present in the snow cover, a mixture model was used which considered brine as the "inclusion dielectric" within a dry snow "host dielectric." When water in liquid phase was present, the model considered the water as the "inclusion dielectric" in a dry snow "host dielectric." Brine free saline snow was treated as an ice inclusion within an air "host dielectric." Details of these models are available elsewhere (Barber *et al.*, 1994; Barber *et al.*, 1995).

Microwave Radiometry

Brightness temperatures were measured with three dual-polarized Russian ATTEX radiometers at 19, 37, and 85 GHz. All measurements were taken on an undisturbed snow surface flanked by the snowpit sampling grid (Figure 2). The Surface Based Radiometer (SBR) system was operated coincident in both time and space with the snow sampling program.

During each data acquisition set, samples were recorded at 5° increments from 20° through 70°. A custom designed software program automatically controlled radiometer operations. The SBR system recorded a voltage, which was then converted to a T_B. Samples were integrated over a 50-second look period, providing an error estimate of less than 1K.

Calibration of the SBR system is based upon linear regression between an Ecosorb® hot load, and cosmic background radiation. Due to the need for clear skies, only ten calibrations were performed over the field season. Consequently, all calibrations (Figure 3a) were averaged into one general calibration equation for each frequency. All voltages were then re-analyzed using this general calibration. It is felt this is the best option to minimize sensor effects which could obscure the results. Relative stability (Figure 3b) also appears adequate. A nonparametric Kruskal-Wallis test confirms that the five sample runs are statistically equivalent.

Emissivities

For a given snow covered sea ice surface, T_B is a function of ice and snow emission: i.e.,

$$T_B(f, \theta_i) = eT_i \qquad (1)$$

where f is frequency, θ_i is the incidence angle, e is the dimensionless emission coefficient ($0<e<1$), and T_i is the physical temperature of the snow-ice combination in Kelvin. In defining a relationship between SWE and T_B, we take advantage of the fact that emissivity decreases with an increase in the reflectivity, or the permittivity (Haykin *et al.*, 1994).

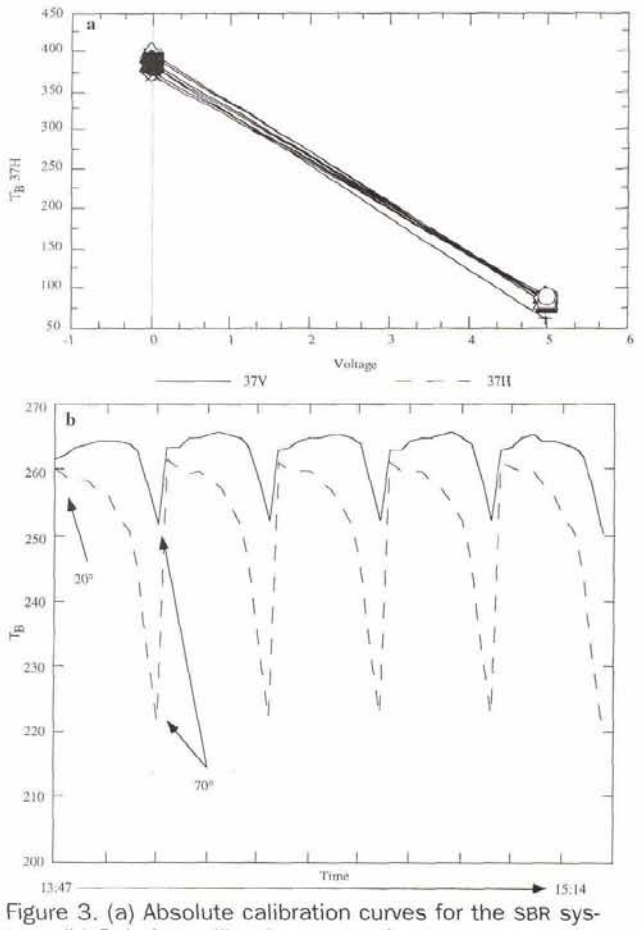

Figure 3. (a) Absolute calibration curves for the SBR system. (b) Relative calibration curves for the SBR system.

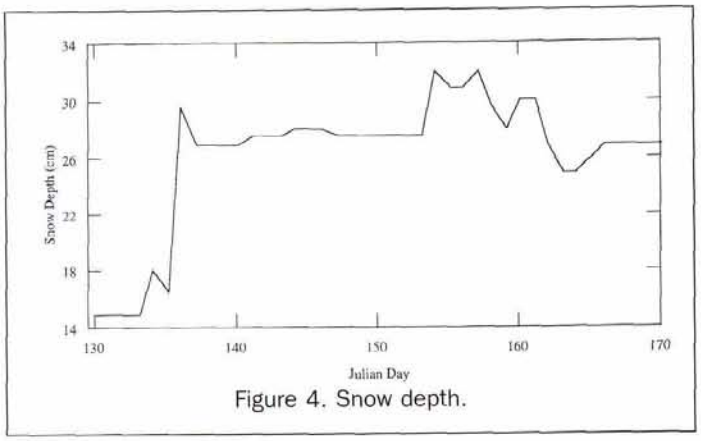

Figure 4. Snow depth.

Results and Discussion

Geophysical Properties

Snow depth was initially 15 cm but quickly rose to near 30 cm, where it fluctuated for the rest of the field project (Figure 4). These fluctuations were mainly a result of the snow being redistributed by wind and storms.

Profile Distributions

Over the field season, the vertical profile of liquid water (Figure 5a) exhibits noticeable increases towards the ice surface. This is a result of increased temperatures and drainage as the spring season advances. Modeled loss values at 37 GHz (Figure 5b) closely correspond to liquid water volumes. This result is expected due to the control which water in liquid phase has on the complex permittivity of snow (Ulaby *et al.*, 1986). A third variable of interest, snow pack density, shows some diversity in the profile (Figure 5c). Densities are highest in the middle layers, and decrease towards the snow-ice boundary as well as the snow-air boundary. New snowfall, with low densities, accounts for the lower values in the upper pack, while the formation of large kinetic growth grains explains the lower densities in the basal layers. Interestingly, results from previous research (e.g., Barber *et al.*, 1995) indicate that the basal layers (1 to 3 in our study) should be significantly less dense than the middle and upper snowpack layers. However, during C-ICE '97, an abnormal amount of ice mass agglomerates were evident in the snowpack, especially in the basal layers. Further, ice lenses, with densities approaching 900 $kg \cdot m^{-3}$, were apparent in the lower three snow layers. Modeled permittivity at 37 GHz (Figure 5d) closely resembles density measurements, due to the influence density has on permittivity. Finally, significant variation in salinity is present in the lower portion of the snowpack, where brine is wicked upwards by capillary suction (Figure 5e).

Seasonal Evolution

Seasonally, the water content remains relatively constant during the first half of the field season and then shows increased variability in the latter half (Figure 6a). As the season progressed towards spring, the incidence of warm storm fronts increased, explaining the larger variance in liquid water. The general increase in the late season is a result of elevated air temperatures corresponding to the spring temperature evolution. Modeled 37-GHz loss values (Figure 6b) do not increase as substantially as liquid water because of the corresponding loss in snow salinity as wetness increases. Both density (Figure 6c) and derived 37-GHz permittivity (Figure 6d) show a slight increase, especially in the upper layers, as the spring progresses. Natural compaction, wind effects, and melt-freeze cycles all increase snowpack density, especially in the uppermost layers. Salinity values decrease slightly as spring advances (Figure 6e), owing to seasonal warming. With warmer temperatures, brine drainage begins, and correspondingly lower salinity concentrations are observed.

Diurnal Variation

Diurnally, a noticeable difference between the three sample sets for liquid water content (Figure 7a) and modeled 37-GHz loss (Figure 7b) becomes clear towards the end of the field project. *Am* water contents remain fairly stable, while *noon* and especially *pm* sets show a rise in liquid water content. Little difference in either density (Figure 7c) or modeled 37-GHz permittivity (Figure 7d) is noted, as expected. Density will change mainly through metamorphism, which is more noticeable over seasonal rather than diurnal scales. Finally, the small observed decrease in salinity (Figure 7e) implies that gravity drainage of water in liquid phase was small over the sampling period.

Microwave Radiometry

Geophysical Effects on SWE Monitoring

Comparison between snow density and microwave brightness temperatures (Table 1) indicates a consistent negative correlation. Increasing densities induce more volume scattering, thereby reducing the T_B.

Disregarding natural variability in snow properties will adversely affect the SWE predictive capabilities of microwave radiometry. If we examine the amount of variability which can be explained by combinations of frequency and polarization, we see that R^2 values display poor results with combined data from *am*, *noon*, and *pm* sets (Figure 8). At H

TABLE 1. CORRELATION MATRIX BETWEEN SNOWPACK LAYERS AND BRIGHTNESS TEMPERATURES

Layer	19H	19V	37H	37V	85H	85V
6	−0.23	−0.23	−0.28	−0.32	−0.30	−0.17
5	−0.08	−0.10	−0.13	−0.09	−0.08	−0.05
4	−0.23	−0.19	−0.17	−0.13	−0.08	−0.07
3	−0.25	−0.18	−0.24	−0.21	−0.20	−0.40
2	−0.25	−0.22	−0.31	−0.30	−0.44	−0.46
1	−0.13	−0.17	−0.31	−0.36	−0.26	−0.29

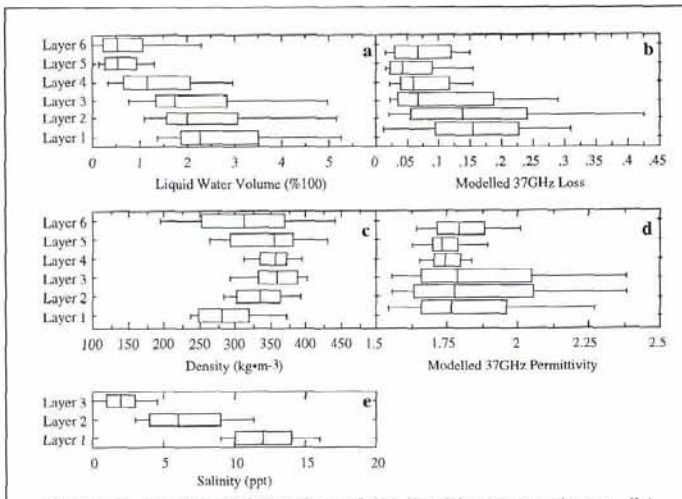

Figure 5. Profile distribution of (a) liquid water volume, (b) modeled 37-GHz loss, (c) density, (d) modeled 37-GHz permittivity, and (e) salinity.

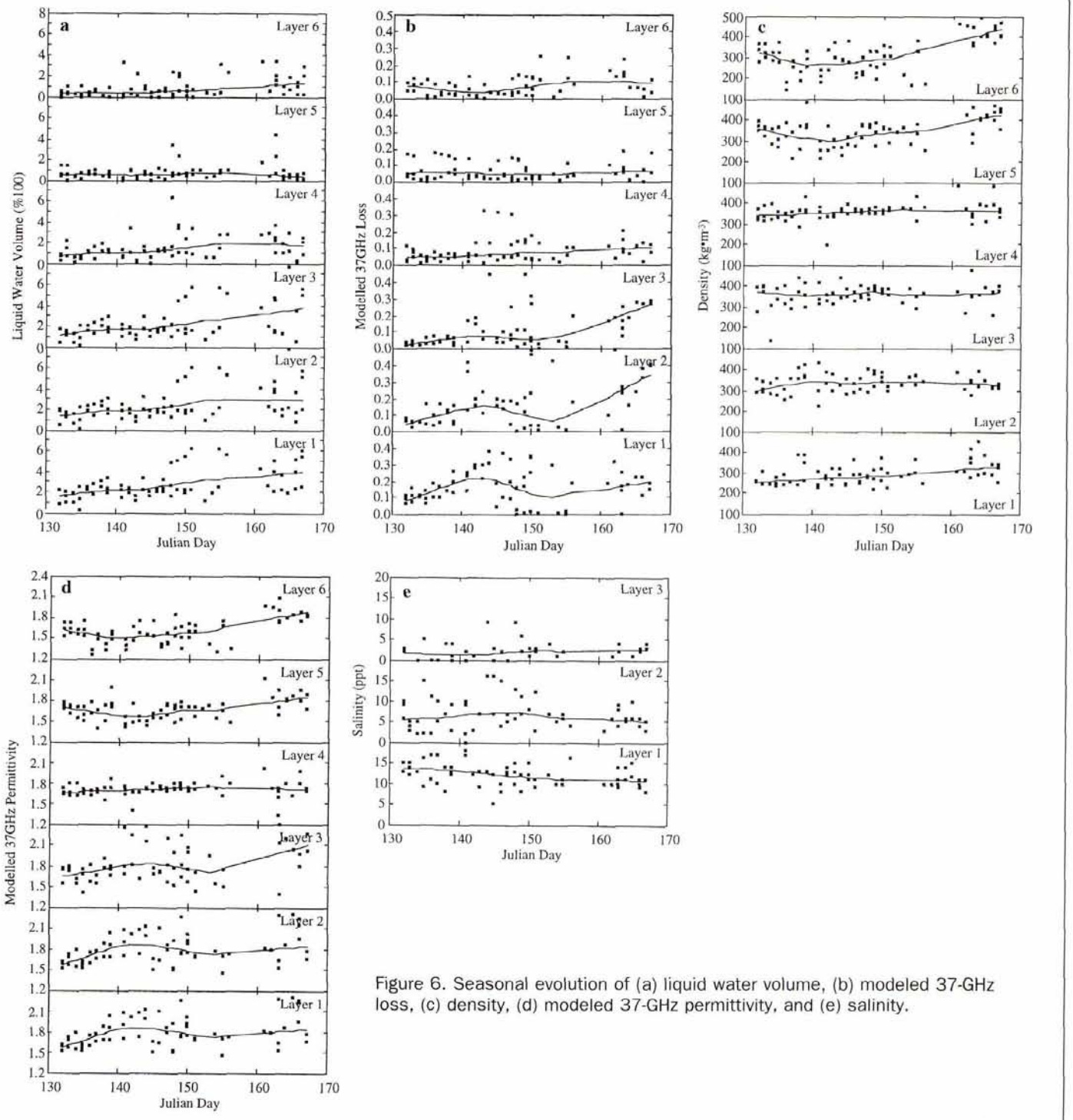

Figure 6. Seasonal evolution of (a) liquid water volume, (b) modeled 37-GHz loss, (c) density, (d) modeled 37-GHz permittivity, and (e) salinity.

polarization, 85-GHz results are the weakest; 37-GHz are strongest. For V polarization, 19 GHz is the poorest estimator, while 85 GHz is best. Nineteen GHz is the least sensitive frequency to changes in the snowpack, and this explains the lower R^2 values. Inversely, 85 GHz is known to be very responsive to slight variations in liquid water content, and this likely weakens the relationship between SWE and T_B at H polarization.

Improving microwave radiometric SWE necessitates understanding sources of confusion, such as liquid water, density, and dielectrics. Recall from Figure 7 that water content and modeled 37-GHz loss were higher in the *noon* and *pm* sets. To further illustrate, the seasonally averaged liquid water volume (Figure 9) clearly displays that the *pm* set has the most free water, followed by *noon* and then *am*.

Subsetting the data into *am*, *noon*, and *pm* sets shows

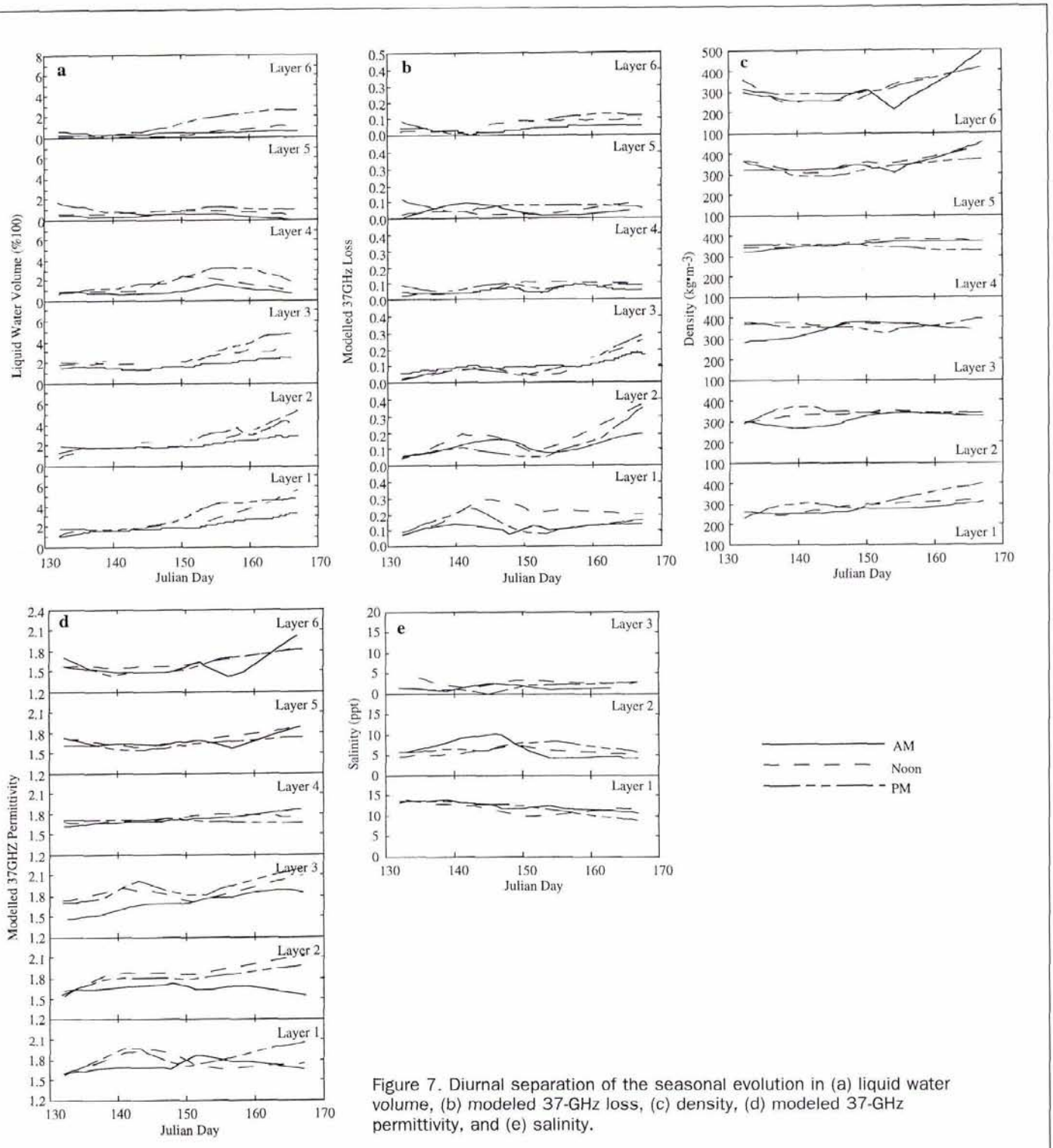

Figure 7. Diurnal separation of the seasonal evolution in (a) liquid water volume, (b) modeled 37-GHz loss, (c) density, (d) modeled 37-GHz permittivity, and (e) salinity.

that *am* data explains a much higher percentage of the observed variability than either *noon* or *pm* results (Table 2). The lower liquid water contents of the *am* set contribute to increasing the SWE predictive capabilities. Note that the lowest R^2 value (*pm*) coincides with the highest liquid water content and dielectric loss values. Dielectrically, the *pm* snowpack is emitting noticeable energy which elevates the brightness temperature, thus lowering the predictive capabilities. The *noon* set, with a slightly lower water content, exhibits a similar effect on a smaller scale. Once the effects of liquid water and dielectric loss are analyzed, SWE prediction from microwave radiometry improves dramatically.

SWE Algorithm Development

Practical SWE prediction includes various combinations of polarization and frequency. Although the initial and subset

analyses use only single frequencies, the majority of SWE retrieval algorithms use a combination of 19 and 37 GHz. Two algorithms, after Chang *et al.* (1987) (Equation 2) and Goodison *et al.* (1990) (Equation 3), are analyzed with *am* data in this study: i.e.,

$$\text{SWE} = K_l(T_{19\text{H}} - T_{37\text{H}}) \tag{2}$$

$$\text{SWE} = \frac{K_l(T_{37\text{V}} - T_{19\text{V}})}{19} + K_z \tag{3}$$

where K_l and K_z are orbital corrections based on geographic location and T_{19x} and T_{37x} are brightness temperatures at a particular frequency and polarization.

Results indicate that neither Equation 2 nor Equation 3 estimate SWE as precisely as 37H or 37V for the conditions observed in this case study (Table 3). This may result from the fact that Equations 2 and 3 were created for terrestrial surfaces, and the physical characteristics of the snow covered sea ice volume are sufficiently different to make Equations 2 and 3 less precise over our case study. Combining V and H polarizations from Equations 2 and 3 shows no improvement over 37H (refinement 1), or a much worse result (refinement 2). Adding 85 GHz to 37 GHz also provides an inferior estimator. Similarly, polarization information is of little value. We speculate that even the smallest amount of liquid water negates the potential of using polarization information or 85 GHz to predict SWE. Simple combinations of frequency and polarization do not improve the SWE predictive ability of microwave radiometry.

Incidence angle effects were examined to see if angular differences provide any improvement in SWE prediction. Results show that angles from 20° through 60° are fairly uniform as SWE estimators (Figure 10). Sixty degrees is the best estimator for three frequencies, while 20°, 30°, and 40° each estimate one frequency the best. However, the differences in R^2 values are not considered statistically distinguishable. Overall, 60° is marginally the best, while 70° is clearly the worst. Varying the incidence angle also appears to be of limited value in SWE prediction. However, the data are too limited to provide a definitive answer as to the most appropriate SWE estimation angle.

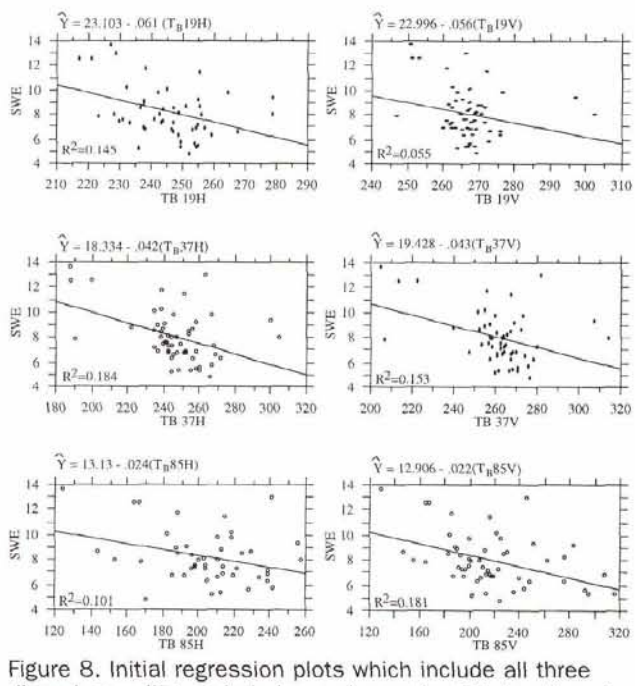

Figure 8. Initial regression plots which include all three diurnal sampling periods lumped over the full duration of the field experiment.

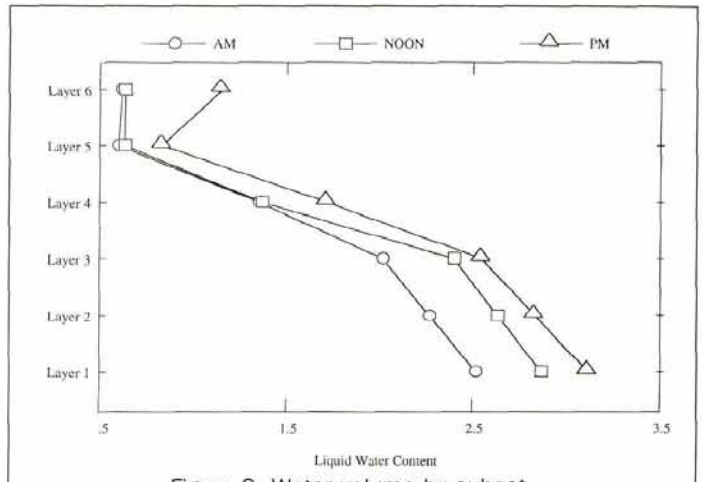

Figure 9. Water volume by subset.

TABLE 2. SUBSETS OF 50° T_B VS. SWE

	R^2		
Frequency	am	noon	pm
19H	0.70	0.27	0.04
19V	0.73	0.26	0.01
37H	0.91	0.34	0.03
37V	0.89	0.27	0.01
85H	0.85	0.38	0.01
85V	0.71	0.32	0.05

TABLE 3. SINGLE AND MULTI-FREQUENCY/POLARIZATION R^2

Variables	R^2	Comments
19H-37H	0.72	Chang *et al.*, 1987
37V-19V	0.89	Goodison *et al.*, 1990
19V-37H	0.90	Refinement 1
19H-37V	0.68	Refinement 2
85V-37V	0.12	85GHz
85H-37H	0.08	85GHz
19V-19H	0.10	Polarization Effect
37V-37H	0.18	Polarization Effect
85V-85H	0.04	Polarization Effect

Multiple regression techniques were also explored to see if any improvement in SWE prediction results. Using all six channels, we found that 96.8 percent of the observed variation could be explained (Table 4). Separating into H polarizations (92.9 percent) and V polarizations (91.5 percent) across all frequencies yields equally good estimators, while 37 GHz (90.7 percent) is slightly better than 19 GHz (89.1 percent) and 85 GHz (85.7 percent). Clearly, the use of multiple regression analysis dramatically improves results. Caution must be noted because the improvement is, at least in part, due to the statistical artifact of increasing the number of independent variables. This given, we still recommend continued research into multivariable approaches to SWE estimation.

Conclusions and Further Research

We have shown that differences in diurnal separation of the seasonal evolution of both snow physical and electrical properties can be exploited in SWE estimation. Increasing the per-

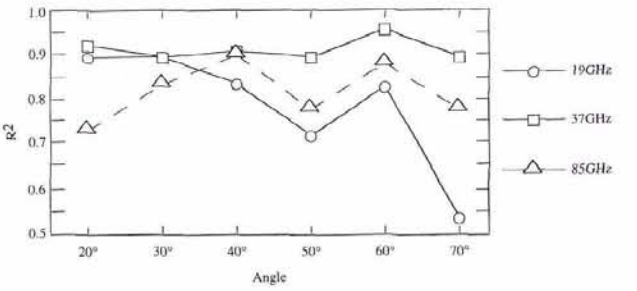

Figure 10. Incidence angle effects on SWE estimation.

TABLE 4. SINGLE AND MULTI-FREQUENCY/POLARIZATION R^2

Variables	R^2	Comments
All Freq/Pol	0.97	Multiple Linear Regression
V Pol	0.92	Multiple Linear Regression
H Pol	0.93	Multiple Linear Regression
19GHz	0.89	Multiple Linear Regression
37GHz	0.91	Multiple Linear Regression
85GHz	0.86	Multiple Linear Regression

mittivity will lower the apparent brightness temperature. Empirical results confirm the link between increasing snowpack density and a decreasing T_B. For SWE estimation with microwave radiometry, 37 GHz is the most precise frequency within the constraints of our case study. Simple frequency or polarization combinations are no better than single channels in simple linear regression analysis, but combining frequencies and/or polarizations provides a better estimator when using multiple regression techniques. Analysis regarding the effect of incidence angle in SWE estimation is shown to be inconclusive at present.

Heterogeneity in the profile observed over the case site has implications for candidate algorithms using spaceborne satellites. Specifically, this study illustrates the effect a diurnal change in liquid water content exhibits in SWE estimation over the case site. Candidate algorithms exploiting spaceborne passive microwave sensors must take into account the overpass time, because the geophysical properties of snow strongly influence SWE estimation over snow covered sea ice.

To pursue the questions analyzed and raised in this paper, future work involves minimizing liquid water effects and assessing the effects of grain size through diurnal sampling. Our results indicate that SWE estimation is more effective when liquid water contents are minimal (cold air temperatures). As a result, further *in situ* research will be undertaken earlier in the year. As well, we will add grain geometry measurements into the diurnal sampling scheme to better understand the influence of grain size and shape. Finally, we will scale up the study by applying these results to SSM/I SWE estimates over sea ice.

Acknowledgments

The authors would like to thank Canadian Ice Services, particularly Ken Asmus, for lending and assisting with the radiometers. Thanks are extended to Cam Grant, Tom Grenfell, and John J. Yackel for data collection and analysis. John Iacozza is given credit for editorial assistance. This study was supported by CRYSYS (B. Goodison, PI), Canadian Ice Services, the Natural Sciences and Engineering Research Council (NSERC), Office of Naval Research (ONR), and the Northern Studies Training Program. Thanks to Polar Continental Shelf for logistical support.

References

Barber, D.G., T.N. Papakyriakou, and E.F. LeDrew, 1994. On the relationship between energy fluxes, dielectric properties, and microwave scattering on snow covered first-year sea ice during the spring transitional period, *Journal of Geophysical Research (Oceans)*, 99(C11):22,401–22,411.

Barber, D.G., S.P. Reddan, and E.F. LeDrew, 1995. Statistical characterization of the geophysical and electrical properties of snow on landfast first-year sea ice, *Journal of Geophysical Research (Oceans)*, 100(C2):2673–2686.

Brown, R.D., and P. Cote, 1992. Interannual Variability of Landfast Ice Thickness in the Canadian High Arctic, 1950–89, *Arctic*, 45: 273–284.

Brown, R.D., and B.E. Goodison, 1993. Recent observed trends and modelled interannual variability in Canadian snow cover, *Proceedings of the 50th Eastern Snow Conference*, Quebec City, pp. 389–397.

Carroll, T.R., 1990. Operational airborne and satellite snow cover products of the national operational hydrologic remote sensing center, *Proceedings of the Forty-Seventh Annual Eastern Snow Conference*, 7–8 June 1989, Vancouver, Canada.

Carsey, F.D., 1992. *Microwave Remote Sensing of Sea Ice*, AGU Geophysical Monograph 68, 462 p.

Chang, A.T.C., P. Gloersen, T. Schmugge, T.T. Wilheit, and H.J. Zwally, 1976. Microwave emission from snow and glacier ice, *Journal of Glaciology*, 16:23–29.

Chang, A.T.C., J.L. Foster, D.K. Hall, A. Rango, and B.K. Hartline, 1982. Snow water equivalent estimation by microwave radiometry, *Cold Regions Science and Technology*, 5:259–267.

Chang, A.T.C., J.L Foster, and D.K. Hall, 1987. Nimbus-7 derived global snow cover parameters, *Annals of Glaciology*, 9:39–44.

Comiso, J.C., Grenfell, T.C., Bell, D.L., Lange, M.A., and S.F. Ackley, 1989. Passive microwave in-situ observations of winter Weddell sea ice, *Journal of Geophysical Research (Oceans)*, 95(C8): 10891–10905.

Cumming, W., 1952. The dielectric properties of ice and snow at 3.2cm, *Journal of Applied Physics*, 23:768–792.

Flato, G.M., and R.D. Brown, 1996. Variability and climate sensitivity of landfast Arctic sea ice, *Journal of Geophysical Research (Oceans)*, 101(C10):25,767–25,777.

Foster, J.L., D.K. Hall, and A.T.C. Chang, 1984. An overview of passive microwave snow research and results, *Reviews of Geophysics and Space Physics*, 22:195–208.

Garrity, C., and B. Burns, 1988. *Electrical and Physical Properties of Snow in Support of BEPERS-88*, Technical Report MWG 88-11, York University, North York, Ontario, 65 p.

Goodison, B.E., 1989. Determination of areal snow water equivalent on the Canadian prairies using passive microwave satellite data, *IGARSS'89. 12th Canadian Symposium on Remote Sensing. Quantitative Remote Sensing: An Economic Tool for the Nineties*, Vancouver, Canada, 10–14 July, 3:1243–1246.

Goodison, B.E., A.E. Walker, and F.W. Thirkettle, 1990. Determination of snow water equivalent on the Canadian prairies using near real-time passive microwave data, *Proceedings of the Workshop on Applications of Remote Sensing in Hydrology, Saskatoon, Canada* (G.W. Kite and A. Wankiewicz, editors), pp. 297–309.

Grenfell, T.G., and A.W. Lohanick, 1985. Variations of the microwave signatures of sea ice during the late spring and early summer near Mould Bay, NWT, *Journal of Geophysical Research (Oceans)*, 90(C3):5063–5073.

Hall, D.K., A.T.C. Chang, and J.L. Foster, 1986. Detection of the depth-hoar layer in the snow-pack of the Arctic coastal plain of Alaska, USA, using satellite data, *Journal of Glaciology*, 32:87–94.

Hallikainen, M., and D.P. Winebrenner, 1992. The physical basis for sea ice remote sensing, *Microwave Remote Sensing of Sea Ice*, (F. Carsey, editor), Geophysical Monograph, 68:29–44.

Haykin, S., E. Lewis, K. Raney, and J.R. Rossiter, 1994. *Remote Sensing of Sea Ice and Icebergs*, John Wiley & Sons, Toronto, 686 p.

Kunzi, K.F., S. Patil, and H. Rott, 1982. Snow-cover parameters retrieved from Nimbus-7 Scanning Multi-Channel Microwave Radiometer (SMMR) data, *IEEE Transactions on Geoscience and Remote Sensing*, GE20:452–467.

Ledley, T.S., 1991. Snow on sea ice: Competing effects in shaping climate, *Journal of Geophysical Research (Atmospheres)*, 96(D9): 17,195–17,208.

———, 1993. Variations in snow on sea ice: A mechanism for producing climate variations, *Journal of Geophysical Research (Atmospheres)*, 98(D6):10,401–10,410.

Lohanick, A.W., 1993. Microwave brightness temperatures of laboratory-grown undeformed first-year ice with an evolving snow cover, *Journal of Geophysical Research (Oceans)*, 98(C3):4667–4674.

Mätzler, C., 1997. Autocorrelation functions of granular media with free arrangement of spheres, spherical shells or ellipsoids, *Journal of Applied Physics*, 81(3):1509–1517.

Rango, A., 1988. Progress in developing an operational snowmelt-runoff forecast model with remote sensing input, *Nordic Hydrology*, 19:65–76.

Rind, D., R. Healy, C. Parkinson, and D. Martinson, 1995. The role of sea ice in 2X CO2 climate sensitivity. Part I: The total influence of sea ice thickness and extent, *Journal of Climate*, 8:449–463.

Ulaby, F.T., R.K. Moore, and A.K. Fung, 1986. *Microwave Remote Sensing: Active and Passive: Volume III: From Theory to Application*, Addison-Wesley Publishing Company, Massachusetts, 1097 p.

Walker, A.E., and B.E. Goodison, 1993. Discrimination of a wet snow cover using passive microwave satellite data, *Annals of Glaciology*, 17:307–311.

(Received 17 April 1997; accepted 22 August 1997; revised 5 November 1997)